De Novo Design and Molecular Dynamics Evaluation of AZ67-Derived Allosteric PFKFB3 Modulators for Anticancer Metabolic Drug Discovery

Aeshah Muhana Mohammed*, Jameelah Kadhim Taher Al-Isawi and Muqdad Khamis Abd

Department of Chemistry, College of Education for Pure Science Ibn Al-Haitham, University of Baghdad, Baghdad, Iraq

Abstract: PFKFB3 is a druggable regulator of fructose-2,6-bisphosphate production, glycolytic flux, angiogenic metabolism, and tumour-cell survival signalling. This study redesigned the AZ67 allosteric scaffold to prioritise computational leads for anticancer metabolic drug discovery. ChemoDOTS enumeration produced 575,760 virtual products and 509,921 standardised unique structures. A reconstructed two-branch workflow applied sequential molecular-weight, lipophilicity, and relaxed drug-like criteria in one branch and PAINS filtering in parallel; intersection with Brenk-alert exclusion retained 10,996 candidates. Five-objective Pareto ranking and diversity filtering selected 50 compounds. A separate six-descriptor AZ67-referenced triage rule identified 27 comparator-qualified candidates but was not interpreted as proof of improved overall drug-likeness. Three nonredundant representatives—MOL_0052111, MOL_0051973, and MOL_0000552—were selected to test distinct substitution hypotheses, followed by docking in the PFKFB3 allosteric pocket (PDB 5AJV), 50-ns molecular dynamics, and MM/GBSA estimation. GNINA outputs were reported according to their distinct conventions: the empirical docking score was interpreted as more favourable when more negative, whereas CNNaffinity was reported on a positive pK scale, with higher values indicating stronger predicted affinity. The selected derivatives had higher molecular weight and topological polar surface area and lower QED than AZ67, although several had lower logP and higher Fsp3. MOL_0000552 gave an empirical docking score of -7.55 kcal/mol and CNNaffinity of 8.18 pK, compared with -4.33 kcal/mol and 4.21 pK for AZ67. It showed the least variable ligand trajectory among the derivatives and an MM/GBSA profile near -65 kcal/mol versus approximately -40 kcal/mol for AZ67. MOL_0051973 was a secondary lead, whereas MOL_0052111 underwent a marked ligand-RMSD shift after approximately 25 ns. MOL_0000552 therefore represents a prioritised computational hypothesis, not a validated PFKFB3 inhibitor. Biochemical activity, isoform selectivity, cellular effects, ADMET properties, and reproducibility in longer replicate simulations require confirmation.

Keywords: PFKFB3, AZ67, cancer metabolism, allosteric modulation, molecular docking, molecular dynamics, MM/GBSA, de novo drug design.

INTRODUCTION

Metabolic reprogramming is a defining feature of malignant progression and supports biosynthesis, redox control, adaptation to hypoxia, and survival under therapeutic pressure [1,2]. The bifunctional enzyme 6-phosphofructo-2-kinase/fructose-2,6-bisphosphatase 3 (PFKFB3) is an important control point because its kinase activity generates fructose-2,6-bisphosphate, a potent allosteric activator of phosphofructokinase-1 and an amplifier of glycolytic throughput [3,4]. PFKFB3 is also implicated in noncanonical processes, including cell-cycle control and DNA-damage responses, which broadens its relevance beyond simple measurement of glycolytic flux [5,6].

The oncology rationale is strengthened by endothelial evidence. PFKFB3-driven glycolysis contributes to vessel sprouting, whereas partial and transient PFKFB3 blockade can reduce pathological angiogenesis without requiring complete metabolic shutdown [7,8]. AZ67 is especially informative for medicinal-chemistry development because it emerged from structure-guided optimisation of a selective PFKFB3 series and occupies a pocket distinct from the conserved ATP cleft [9]. Subsequent studies reported that AZ67 can alter angiogenic behaviour through mechanisms that are not explained solely by bulk glycolysis inhibition [10], while allosteric interference can also influence the balance between kinase and bisphosphatase functions [11]. PFKFB3 also contributes to nonmalignant neural physiology, reinforcing the need for tissue-context, selectivity, and safety assessment [12]. These observations support the search for allosteric modulators rather than assuming that every computationally favourable analogue will operate as a conventional orthosteric inhibitor.

PFKFB3 chemical biology already includes several distinct lineages. PFK15 arose from a non-AZ67 scaffold and established preclinical evidence for targeting this metabolic node [13]. KAN0438757/ KAN0438241 provided a separate, experimentally validated inhibitor class with structural and cellular target-engagement data [14]. Clinical exploration of the

*Address correspondence to this author at the Department of Chemistry, College of Education for Pure Science Ibn Al-Haitham, University of Baghdad, Baghdad, Iraq; Email: aeshah.m.m@ihcoedu.uobaghdad.edu.iq

ISSN: 1929-2260 / E-ISSN: 1929-2279/26

related PFK-158 programme established an early translational precedent in advanced solid tumours [15]. More recently, covalent PFKFB3 inhibitors have expanded the targetable chemical space and demonstrated activity in pancreatic ductal adenocarcinoma models [16]. Patent literature also discloses broad PFKFB3-modulator families, including phthalimide and isoindolinone derivatives and known inhibitors such as AZ67 [17]. Consequently, computational novelty must be defined through a specific structure-activity hypothesis, not merely by generating a large virtual library; formal patentability and freedom-to-operate require a dedicated legal and chemical search.

Increasing molecular saturation and Fsp3 is a recognised medicinal-chemistry strategy for reducing excessive molecular flatness, although it does not guarantee developability [18]. The present study used the AZ67 scaffold as a structurally anchored seed and explored three derivatisation regions through reaction-driven enumeration. The objective was to identify nonredundant analogues that preserved a plausible allosteric binding mode while testing whether increased three-dimensionality, altered lipophilicity, and new polar interaction vectors could improve the integrated computational profile. Particular attention was given to transparent reconstruction of the filtration pathway, explicit separation of Pareto objectives from the later six-descriptor triage rule, and cautious interpretation of docking, molecular dynamics, and MM/GBSA outputs. The study is entirely computational; the term modulator is therefore used instead of inhibitor unless referring to experimentally characterised compounds from the literature.

MATERIALS AND METHODS

Study Design

This structure-based in silico study comprised reaction-driven library enumeration, standardisation and deduplication, physicochemical and structural-alert filtering, multi-objective prioritisation, selection of three chemically distinct representatives, docking in the AZ67-defined PFKFB3 allosteric pocket, all-atom molecular dynamics, trajectory analysis, and MM/GBSA estimation. No human participants, animals, biological specimens, or clinical records were used.

De Novo Library Construction

AZ67 was used as the seed because of its crystallographically characterised interaction with PFKFB3 [9]. Derivatisation vectors were assigned to the amide, arylnitrile, and secondary alkylamine regions following contemporary de novo-design principles [19]. ChemoDOTS was used to construct chemistry-driven focused libraries [20], drawing on robust reaction rules described for in silico molecule design [21]. The reaction set included reductive amination, Niementowski quinazoline synthesis, Schotten-Baumann amide formation, and additional transformations supported by the enumeration platform. Three combinatorial cycles applied to 501,542 building blocks produced 575,760 virtual products.

Standardisation and Reconstructed Filtration Pathway

Enumerated structures were desalted, neutralised, canonicalised, and deduplicated, leaving 509,921 standardised unique molecules. The filtration logic was reconstructed as two branches because the PAINS-clean count was generated from the standardised library rather than from the smaller relaxed drug-like subset. In the physicochemical branch, compounds were first restricted to molecular weight ≤600 Da (n=47,041), then to calculated logP ≤6.0 (n=29,884), and then to a relaxed drug-like subset (n=14,392) informed by oral-bioavailability principles [22]. In parallel, the standardised library was evaluated with PAINS filters [23], yielding 362,974 PAINS-clean structures. The intersection of the relaxed drug-like branch with structural-alert-clean criteria, including Brenk-alert exclusion [24], produced the final clean pool of 10,996 candidates. Table **1** and Figure **1B** present the parent set for every step so that the pathway is not misread as a single sequential cascade.

Multi-Objective Ranking and Six-Descriptor Triage Rule

The 10,996-compound pool was ranked by nondominated sorting following NSGA-II principles [25]. Five minimised objectives were used: molecular weight, logP, 1-QED, 1-Fsp3, and absolute TPSA deviation from AZ67. QED served as an integrated descriptor rather than a measured developability endpoint [26]. Fingerprint-based Tanimoto similarity was used to reduce redundancy [27], and 50 structurally diverse candidates were retained.

A separate descriptive comparator was then applied to the top-50 set. Six axes were included: molecular weight, logP, QED, Fsp3, hydrogen-bond donor count (HBD), and TPSA. For this operational triage rule, lower molecular weight, logP, HBD, and TPSA and

higher QED and Fsp3 were counted as directionally favourable relative to AZ67. Compounds meeting at least three of the six directional rules were designated comparator-qualified (n=27). This post-ranking heuristic was not a sixth Pareto objective and was not interpreted as proof of superior global drug-likeness, oral bioavailability, or pharmacokinetics.

Selection of Three Representatives

Three compounds were selected from the comparator-qualified group as nonredundant representatives of distinct substitution hypotheses rather than as the first three entries of a single-score ranking. MOL_0052111 combined the highest Fsp3 among the three selected compounds (0.33) with lower logP than AZ67 and represented the N-acetyl-dimethylamino branch. MOL_0051973 had the highest QED (0.39) and composite selection score (0.2075) among the three and represented an N-methylcarbamoyl/urea interaction hypothesis. MOL_0000552 had the lowest logP (4.09), a strong composite score (0.2000), and an N-methyl-tetrazole substituent that tested an expanded polar-interaction vector. This design enabled direct comparison of complementary property trade-offs and dynamic behaviour (Table **2**; Figure **5**).

Protein Preparation and Molecular Docking

The human PFKFB3 kinase-domain structure was obtained from the Protein Data Bank (PDB ID 5AJV) [28], using the co-crystallised AZ67 site to define the allosteric pocket [9]. Crystallographic water molecules and the reference ligand were removed during receptor preparation. Three-dimensional ligand conformers were generated and MMFF94 charges were assigned [29]. Docking was performed with GNINA, which combines an empirical docking function with convolutional-neural-network models [30,31]. Two output fields were retained for reporting: the empirical energy-like docking score, for which more negative values were interpreted as more favourable, and CNNaffinity, which was reported on GNINA's positive pK scale, for which higher values indicate stronger predicted affinity. The CNN pose-classification score was not used for ranking. AZ67 was retained as the reference comparator.

All-Atom Molecular Dynamics Simulations

Separate PFKFB3 complexes were prepared for AZ67, MOL_0052111, MOL_0051973, and MOL_0000552. Simulations were conducted in the Desmond environment [32]. Each complex was placed in an orthorhombic box with SPC water and a 10 Å buffer from the protein surface [33]. Systems were neutralised with counterions and parameterised with OPLS4 [34]. After relaxation, a 50-ns production trajectory was analysed for each complex in the NPT ensemble. Temperature was maintained at 300 K with a Nose-Hoover chain thermostat [35], and pressure was maintained at 1.01325 bar with a Martyna-Tobias-Klein barostat [36]. No replicate-trajectory analysis was available in the reported dataset.

Trajectory and MM/GBSA Analyses

Protein-backbone RMSD and protein-aligned ligand heavy-atom RMSD were used to describe global drift and ligand rearrangement. Per-residue RMSF was calculated to identify flexible regions. Ligand radius of gyration, solvent-accessible surface area (SASA), and polar surface area (PSA) were used to describe compactness and solvent exposure [37]. MM/GBSA estimates were calculated from trajectory snapshots as comparative energetic summaries [38]. Because snapshots from the same trajectory are temporally correlated and independent simulation replicates were not available, the box plots in Figure **7B** are descriptive distributions; no hypothesis-test p-values or confidence intervals were inferred.

Chemical-Space Visualisation and Integrated Prioritisation

Uniform Manifold Approximation and Projection (UMAP) was used to display the location of prioritised candidates within the enumerated chemical space [39]. Integrated prioritisation considered descriptor trade-offs, structural diversity, empirical docking score, CNNaffinity, interaction patterns, trajectory behaviour, and MM/GBSA estimates rather than selecting a lead from any single metric [40].

RESULTS

Library Construction and Filtration

The three-cycle enumeration generated 575,760 AZ67-derived virtual products. Standardisation and deduplication retained 509,921 unique structures. In the physicochemical branch, the molecular-weight restriction retained 47,041 structures, the combined molecular-weight/logP criteria retained 29,884, and the relaxed drug-like step retained 14,392. The independent PAINS-clean branch contained 362,974 structures. Intersection of the branches with Brenk-alert exclusion produced 10,996 candidates. Pareto ranking

and diversity filtering retained 50 compounds, of which 27 met at least three of the six AZ67-referenced directional rules (Table **1**; Figure **1**).

Physicochemical Profile and Selection Trade-Offs

The top-50 set did not show uniformly improved drug-like descriptors. Mean molecular weight increased

Table 1: Reconstructed Library-Filtration and Prioritisation Pathway

Stage	Parent set / logic	Candidates (n)	Mean MW	Mean logP	Mean QED	Mean Fsp3	Mean TPSA
Enumerated virtual products	Reaction-driven enumeration	575,760	—	—	—	—	—
Standardised unique library	Enumerated products after standardisation and deduplication	509,921	672.48	6.70	0.16	0.29	143.35
MW ≤600 Da	Standardised library; physicochemical branch	47,041	582.41	5.65	0.21	0.31	130.50
MW/logP filtered	MW ≤600 Da, then logP ≤6.0	29,884	581.07	5.10	0.22	0.30	139.29
Relaxed drug-like subset	MW/logP-filtered set	14,392	576.52	5.42	0.23	0.31	126.74
PAINS-clean branch	Standardised library; parallel structural-alert branch	362,974	669.75	6.70	0.17	0.29	142.07
Relaxed + structural-alert clean	Intersection of relaxed drug-like and PAINS-clean branches, with Brenk-alert exclusion	10,996	577.27	5.44	0.24	0.32	126.94
Top-50 set	Five-objective Pareto ranking + diversity filtering	50	543.60	4.62	0.33	0.35	118.90
Comparator-qualified set	Top-50 candidates meeting ≥3 of the 6 directional AZ67 rules	27	542.81	4.84	0.33	0.35	114.90
AZ67 seed	Reference comparator	1	455.52	4.65	0.44	0.27	105.11

Abbreviations: Fsp3, fraction of sp3 carbons; MW, molecular weight; PAINS, pan-assay interference compounds; QED, quantitative estimate of drug-likeness; TPSA, topological polar surface area. The PAINS-clean count was generated from the standardised library in parallel, not after the relaxed drug-like row.

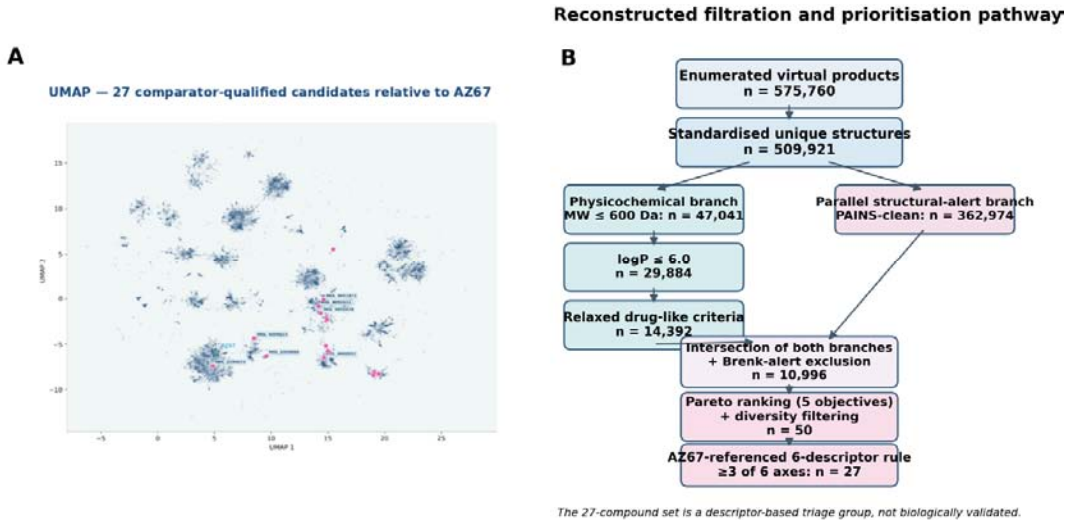

Figure 1: Chemical-space mapping and reconstructed prioritisation of AZ67-derived candidates. (**A**) UMAP projection showing the distribution of comparator-qualified candidates relative to AZ67. Pink points indicate compounds meeting at least three of the six directional AZ67-referenced descriptor rules; this classification does not establish biological activity. (**B**) Reconstructed two-branch filtration logic. The physicochemical/drug-like branch and the parallel PAINS-clean branch were intersected with Brenk-alert exclusion to obtain 10,996 clean candidates, followed by five-objective Pareto ranking, diversity filtering, and the separate six-descriptor triage rule.

from 455.52 Da for AZ67 to 543.60 Da, mean TPSA increased from 105.11 to 118.90 Å², and mean QED decreased from 0.44 to 0.33. In contrast, mean logP decreased slightly from 4.65 to 4.62, and mean Fsp3 increased from 0.27 to 0.35. Within the top-50 set, 31 compounds (62%) had lower logP and 49 (98%) had higher Fsp3 than AZ67; none had lower molecular weight or higher QED under the operational comparator, 25 (50%) had lower HBD, and 13 (26%) had lower TPSA (Figures **2** and **3**). These results indicate a shift towards lower lipophilicity and greater three-dimensionality, offset by higher size/polarity and lower integrated QED.

The same trade-offs were evident in the three selected representatives. MOL_0052111 had molecular weight 540.62 Da, logP 4.45, QED 0.35, Fsp3 0.33, and TPSA 116.63 Å². MOL_0051973 had molecular weight 512.57 Da, logP 4.70, QED 0.39, Fsp3 0.29, and TPSA 125.42 Å². MOL_0000552 had molecular weight 551.61 Da, logP 4.09, QED 0.30, Fsp3 0.31, and TPSA 139.92 Å² (Table **2**). Thus, MOL_0000552

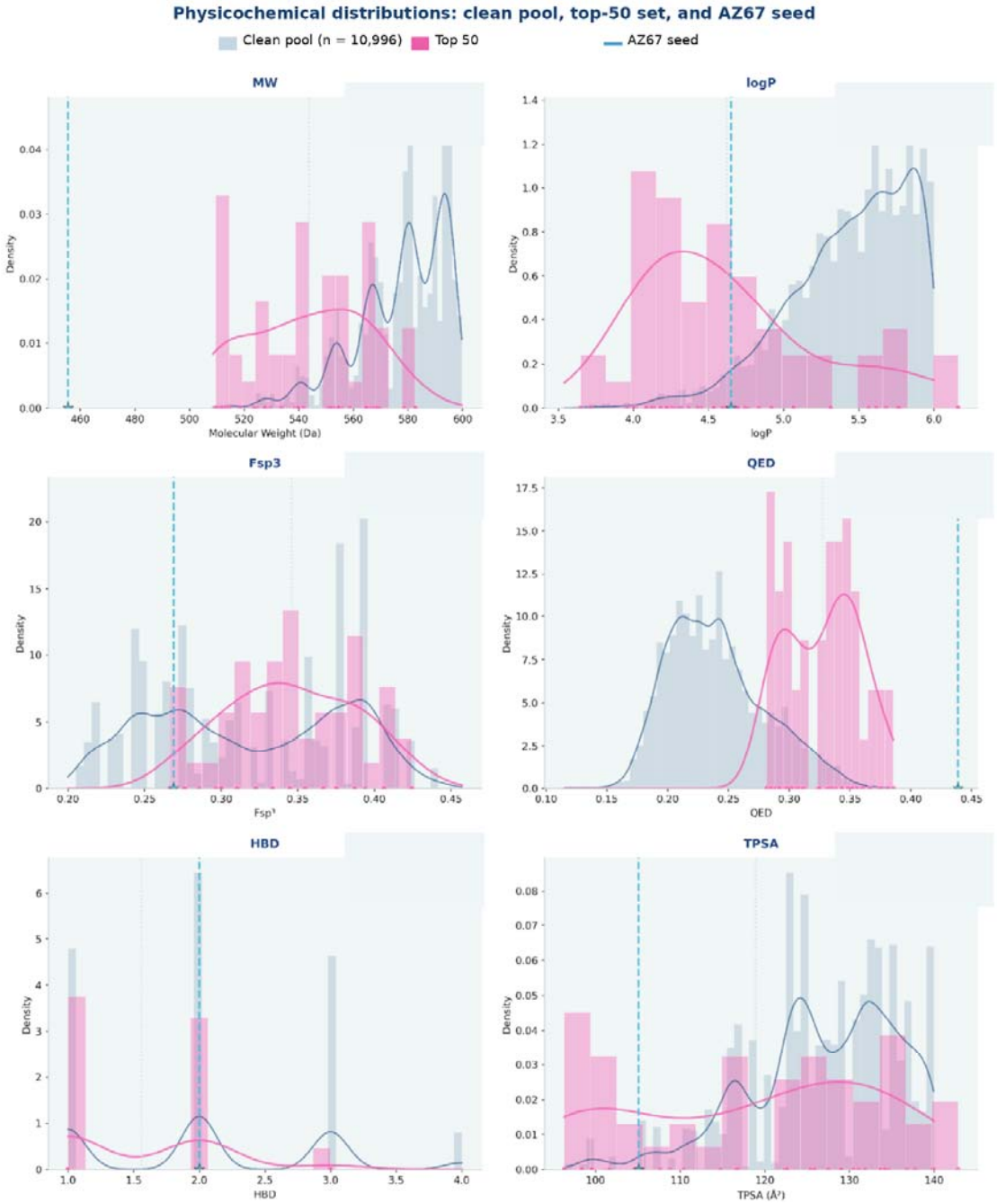

Figure 2: Physicochemical distributions of the clean pool and top-50 set relative to the AZ67 seed. Panels show molecular weight, logP, Fsp3, QED, hydrogen-bond donor count, and TPSA. The figure is descriptive and demonstrates both improvements and trade-offs; the top-50 set was not uniformly superior to AZ67.

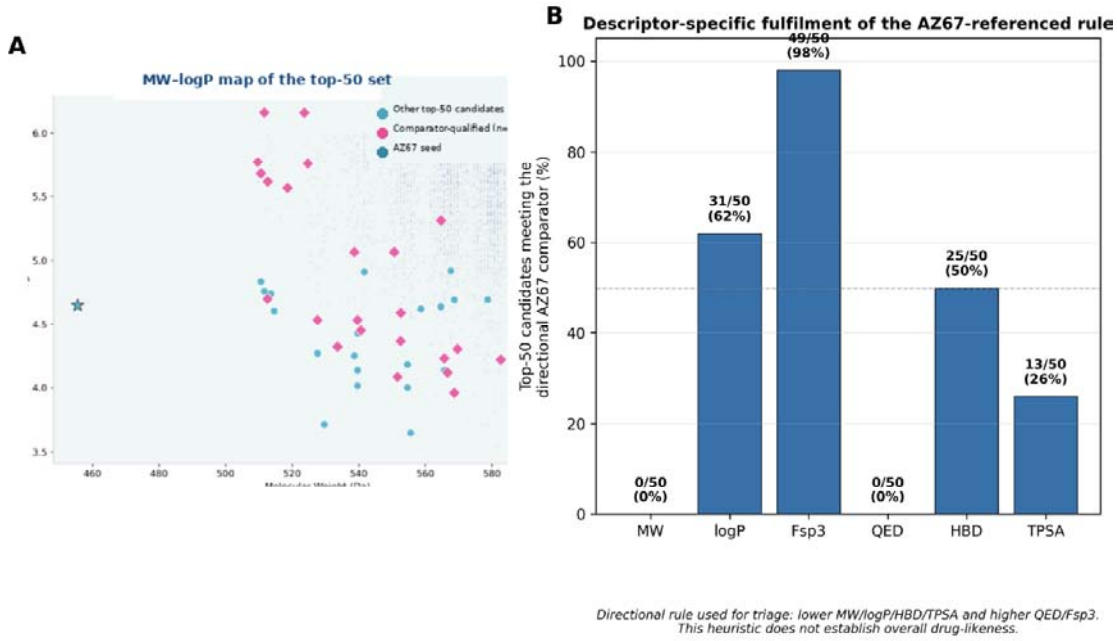

Figure 3. AZ67-referenced descriptor triage within the top-50 set. (**A**) Molecular-weight and logP distribution, with the 27 comparator-qualified candidates distinguished from the remaining 23 compounds. (**B**) Number and proportion of candidates meeting the directional rule for each descriptor. Lower molecular weight, logP, HBD, and TPSA and higher QED and Fsp3 were counted for this operational comparator; the rule does not establish overall drug-likeness.

Table 2: Chemical-Property Profile and Rationale for Selection of the Three Representative Derivatives

Compound	Modification	MW (Da)	logP	QED	Fsp3	TPSA	Composite score	Selection rationale
AZ67	Seed scaffold	455.52	4.65	0.44	0.27	105.11	0.1330	Reference comparator
MOL_0052111	N-acetyl-dimethylamino	540.62	4.45	0.35	0.33	116.63	0.1700	Highest Fsp3 among the three; lower logP; distinct amine-containing branch
MOL_0051973	N-methylcarbamoyl/urea	512.57	4.70	0.39	0.29	125.42	0.2075	Highest QED and composite score among the three; urea interaction hypothesis
MOL_0000552	N-methyl-tetrazole	551.61	4.09	0.30	0.31	139.92	0.2000	Lowest logP; tetrazole interaction hypothesis; increased TPSA trade-off

The three derivatives were selected as nonredundant representatives of complementary substitution and descriptor profiles, not as the first three compounds in a single-metric ranking.

provided the strongest lipophilicity reduction but also the largest TPSA penalty, while MOL_0051973 retained the most favourable QED among the three but did not improve logP relative to AZ67.

Docking Outputs under GNINA Scoring Conventions

AZ67 produced an empirical docking score of -4.33 kcal/mol and CNNaffinity of 4.21 pK. The selected derivatives gave more favourable predictions in both reported fields. MOL_0000552 produced an empirical score of -7.55 kcal/mol and the highest CNNaffinity, 8.18 pK. MOL_0051973 gave -5.65 kcal/mol and 8.17 pK, and MOL_0052111 gave -5.78 kcal/mol and 7.62 pK (Table **3**). MOL_0000552 and MOL_0051973 were therefore almost indistinguishable by CNNaffinity, whereas the empirical score favoured MOL_0000552. These values are model outputs and were not converted into experimental dissociation constants.

Predicted Interaction Profiles

AZ67 occupied the allosteric cleft with contacts involving His243, Met240, Glu381, Arg379, and Gly219 (Figure **4A**). MOL_0052111 preserved predicted contacts with His243, Arg379, and Gly219 and

Table 3: Integrated Prioritisation Using GNINA Scoring Conventions

Compound	Chemical profile	Empirical docking score (kcal/mol)[1]	CNNaffinity (pK)[2]	Molecular-dynamics interpretation	Approximate MM/GBSA profile	Integrated interpretation
AZ67	MW 455.52; logP 4.65; QED 0.44; Fsp3 0.27; TPSA 105.11	-4.33	4.21	Reference trajectory; ligand RMSD approximately 5-13 Å	~ -40 kcal/mol	Reference comparator
MOL_0000552	MW 551.61; logP 4.09; QED 0.30; Fsp3 0.31; TPSA 139.92	-7.55	8.18	Least variable derivative trajectory; does not prove retention of starting pose	~ -65 kcal/mol; most favourable	Primary computational lead for experimental testing
MOL_0051973	MW 512.57; logP 4.70; QED 0.39; Fsp3 0.29; TPSA 125.42	-5.65	8.17	Early rearrangement followed by plateau near 15 Å	~ -45 kcal/mol	Secondary computational lead
MOL_0052111	MW 540.62; logP 4.45; QED 0.35; Fsp3 0.33; TPSA 116.63	-5.78	7.62	Major ligand-RMSD transition after ~25 ns; possible reorientation/displacement	No clear advantage over AZ67 after MD	Docking hit downgraded after dynamic evaluation

[1]More negative is interpreted as more favourable for the energylike empirical docking score. [2]CNNaffinity is reported on GNINA's positive pK scale; higher is interpreted as stronger predicted affinity. MM/GBSA values are comparative approximations, not experimental affinities.

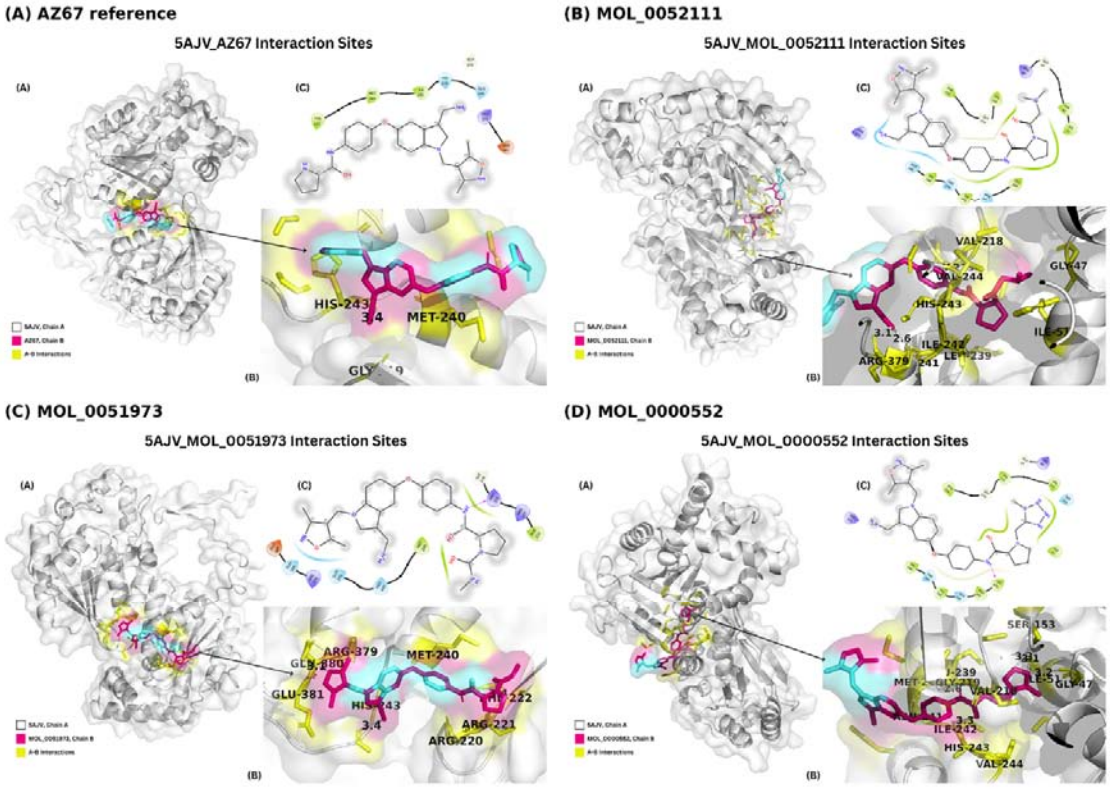

Figure 4: Comparative predicted interaction profiles of AZ67 and selected derivatives in the PFKFB3 allosteric pocket. (**A**) AZ67. (**B**) MOL_0052111. (**C**) MOL_0051973. (**D**) MOL_0000552. Interaction diagrams are docking-derived hypotheses rather than experimentally validated binding modes.

extended towards Val244, Ile242, Asn241, Leu239, Tyr50, Ile51, Gly47, and Arg46 (Figure **4B**). MOL_0051973 introduced an N-methylcarbamoyl/urea group and was predicted to add contacts with Gln380, Gln245, Arg220, Arg221, and Phe222 while retaining interactions near His243, Met240, Glu381, and Arg379 (Figure **4C**). MOL_0000552 generated the broadest predicted interaction network, retaining the His243/Met240/Arg379 region and extending towards Val244, Ile242, Asn241, Leu239, Val218, Phe222,

Ser153, Ile51, Gly47, and Arg46 (Figure **4D**). These interaction maps support substituent-specific hypotheses but do not establish residence time or biochemical activity.

Molecular-Dynamics Behaviour

Protein-backbone RMSD remained within approximately 2-5 Å across the four systems, suggesting no gross unfolding during the 50-ns trajectories. Ligand RMSD distinguished the derivatives more clearly (Figure **6**). AZ67 and MOL_0000552 fluctuated within an approximately 5-13 Å range, with MOL_0000552 showing the least variable trajectory among the derivatives. MOL_0051973 underwent an early rearrangement and then plateaued near 15 Å; this plateau indicates a relatively persistent rearranged state but should not be equated with retention of the starting pose. MOL_0052111 showed a pronounced transition after approximately 25 ns, with ligand RMSD increasing from around 10 Å to above 30 Å, consistent with major reorientation or partial displacement from the pocket. RMSF profiles did not indicate marked destabilisation of the kinase-domain core. Radius of gyration, PSA, and SASA were comparatively steady for AZ67, MOL_0000552, and MOL_0051973, whereas MOL_0052111 showed transiently increased solvent exposure during its RMSD transition.

MM/GBSA Comparison and Lead Prioritisation

The MM/GBSA time series placed MOL_0000552 at the most favourable end of the comparison, with estimates centred near -65 kcal/mol compared with approximately -40 kcal/mol for AZ67. MOL_0051973 was centred near -45 kcal/mol. MOL_0052111 did not retain an energetic advantage over AZ67 after its conformational shift. Energy-component summaries suggested that van der Waals and Coulombic terms were major favourable contributors, particularly for MOL_0000552 (Figure **7**). Because these data arise from correlated snapshots of single trajectories, the

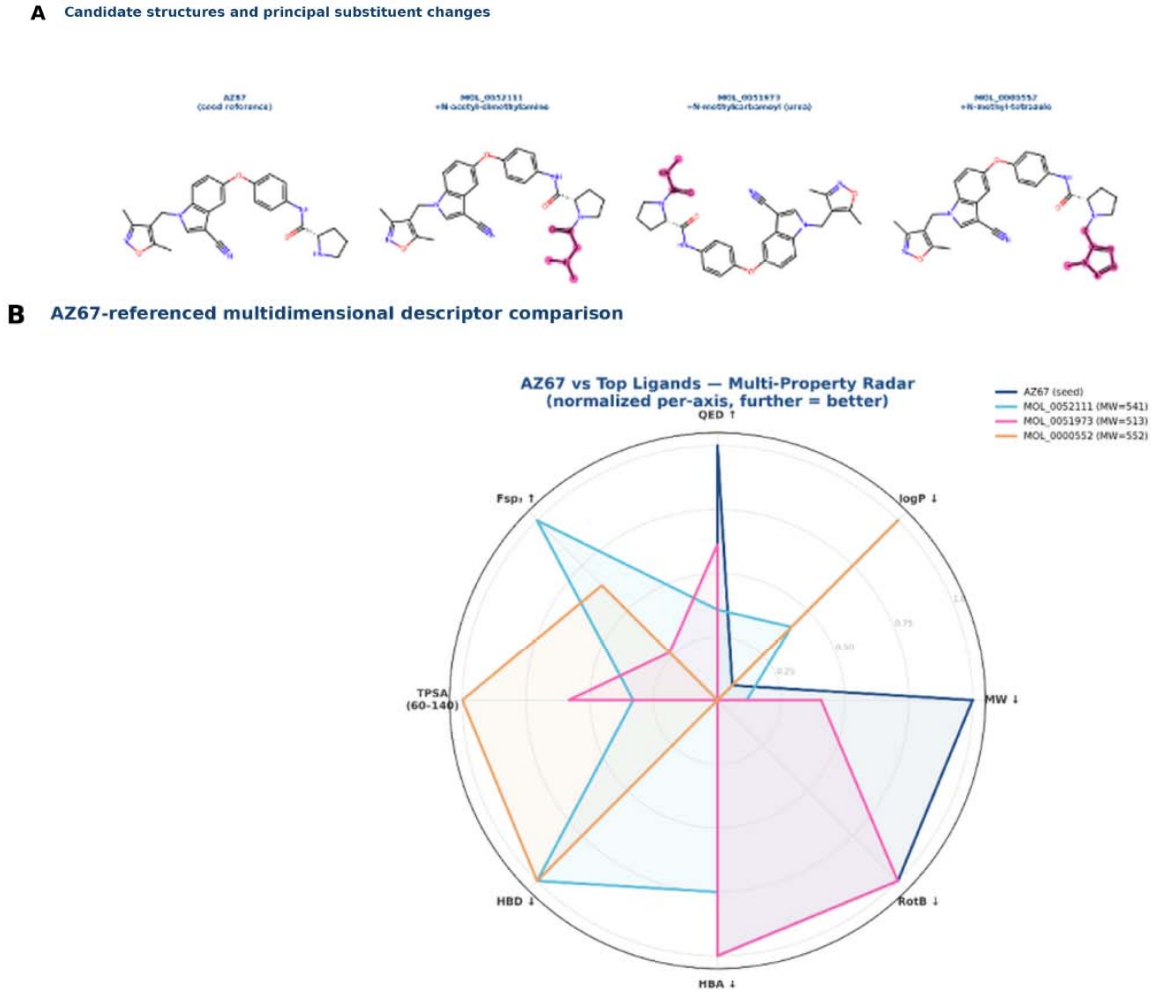

Figure 5: Structural and descriptor comparison of the selected derivatives. (**A**) AZ67 and three nonredundant substituent hypotheses. (**B**) Direction-normalised radar plot illustrating descriptor trade-offs. The axis arrows define the operational direction used for display; distances from the centre should not be interpreted as measured pharmacokinetic performance.

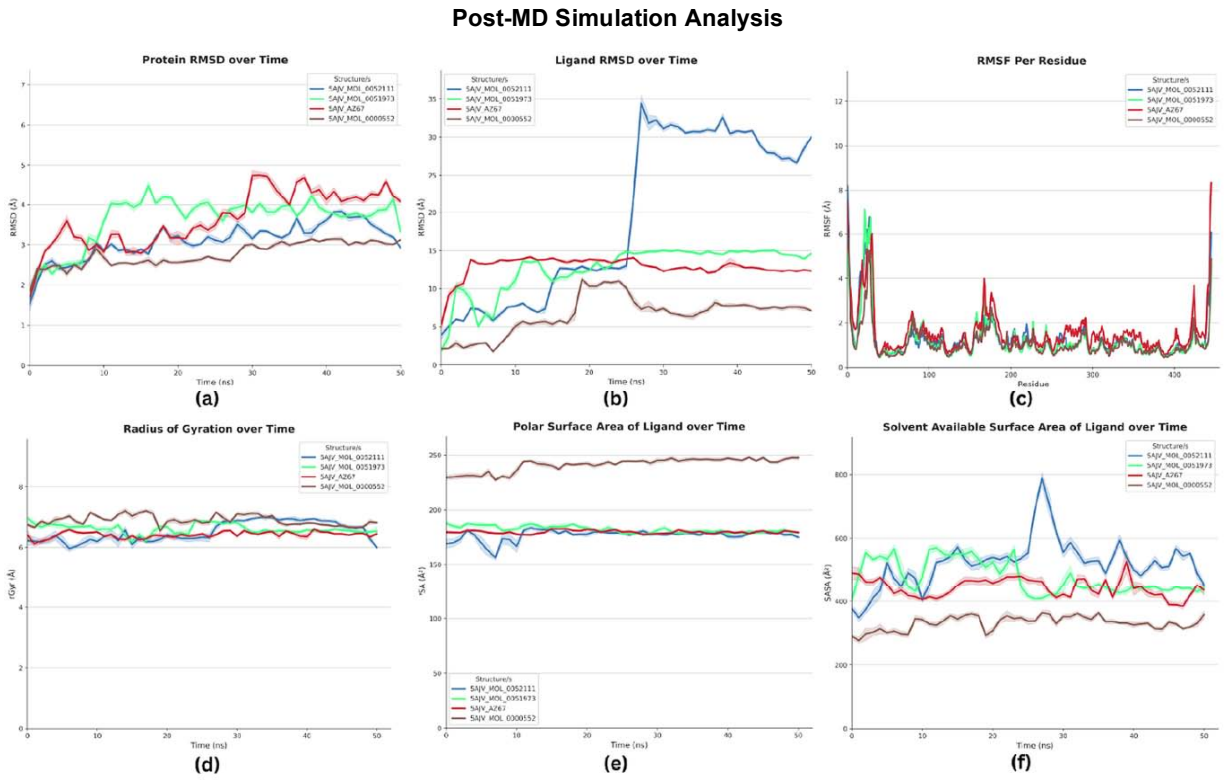

Figure 6: Post-molecular-dynamics trajectory analysis over 50 ns. Panels show protein RMSD, protein-aligned ligand RMSD, residue RMSF, ligand radius of gyration, ligand polar surface area, and ligand solvent-accessible surface area. Ligand RMSD values are interpreted comparatively and do not prove retention of the initial docking pose.

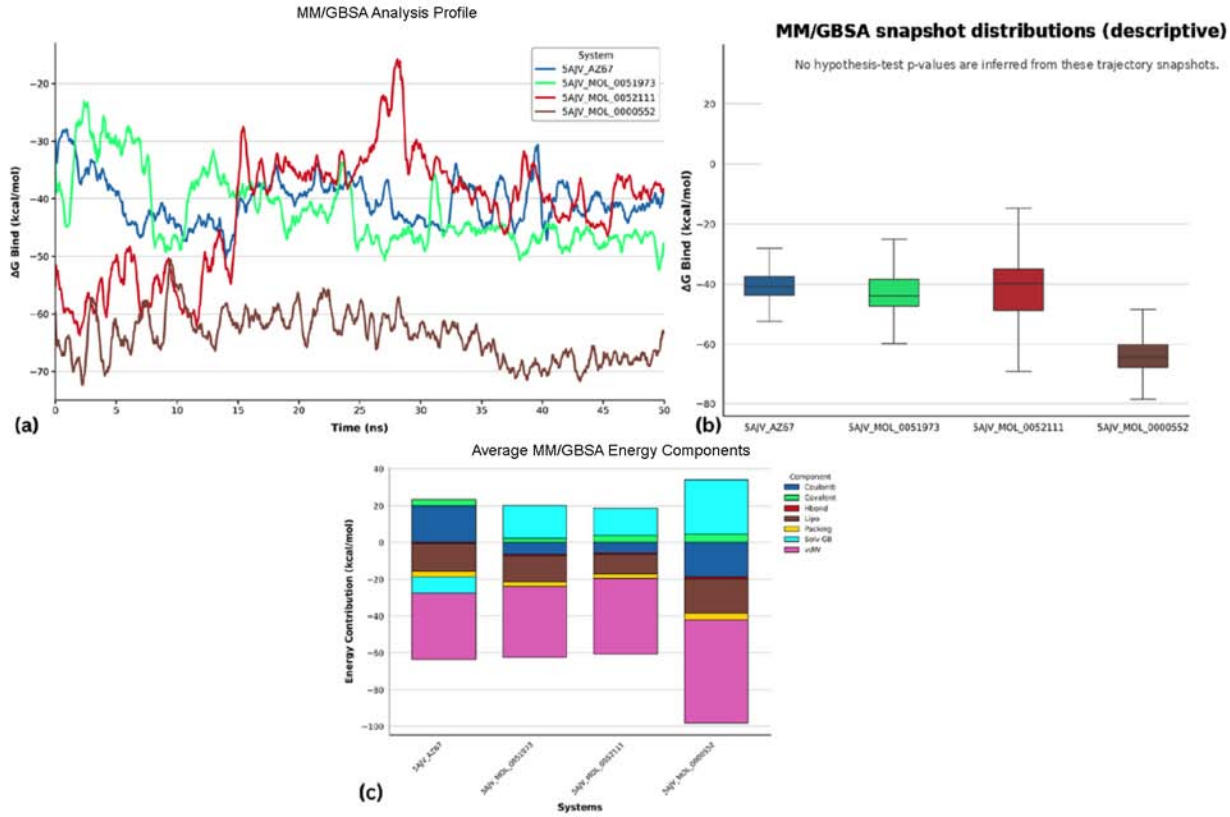

Figure 7: MM/GBSA analysis of AZ67 and selected derivatives. Panels show (**A**) trajectory-snapshot binding-energy estimates, (**B**) descriptive snapshot distributions without hypothesis-test p-values, and (**C**) average energy-component summaries. MM/GBSA values are comparative approximations and not experimental affinities.

apparent separation was treated descriptively rather than as inferential evidence of a statistically significant affinity difference. Integrated interpretation prioritised MOL_0000552, with MOL_0051973 as a secondary computational lead (Table **3**).

DISCUSSION

The present study clarifies both the value and the limits of the computational workflow. The principal result is not that every selected analogue is more drug-like than AZ67; rather, the workflow identified molecules with different trade-offs and then used docking, dynamics, and approximate energetics to distinguish candidates within that constrained chemical space. MOL_0000552 combined the lowest logP among the three selected compounds, a broad predicted interaction network, the strongest empirical docking score, the highest CNNaffinity, the least variable derivative trajectory, and the most favourable MM/GBSA profile. These convergent signals support its prioritisation for testing, but none establishes PFKFB3 inhibition; docking-score generalisability remains target- and chemotype-dependent [41].

The selected compounds extend an experimentally grounded AZ67 scaffold rather than introducing an unrelated chemotype. Boyd and colleagues used structure-guided optimisation to develop potent, selective PFKFB3 inhibitors and provide the structural basis for AZ67 binding [9]. Macut and colleagues subsequently showed that allosteric interference can tune the balance of PFKFB3 activities [11], and AZ67 has shown anti-angiogenic effects not reducible to simple glycolysis inhibition [10]. Relative to that literature, the present medicinal-chemistry hypothesis is that solvent-exposed or pocket-adjacent AZ67 vectors can accommodate more sp3-rich or polar substituents while preserving the His243/Met240/Arg379 interaction region. This hypothesis is more specific—and more testable—than a general claim of improved drug-likeness.

The three substitutions generated different structure-dynamics relationships. The N-methyl-tetrazole analogue MOL_0000552 reduced predicted lipophilicity and expanded the polar interaction network, consistent with the use of heteroaromatic bioisosteres to alter recognition and metabolic liability [42]. The same change increased TPSA to 139.92 Å² and reduced QED, signalling a potential permeability and exposure penalty that must be measured rather than assumed. The N-methylcarbamoyl/urea analogue MOL_0051973 retained the best QED of the three selected compounds and added predicted contacts near Gln380/Gln245 and Arg220/Arg221; amide and urea replacements are established ways to alter geometry and hydrogen-bonding patterns [43]. Conversely, the N-acetyl-dimethylamino analogue MOL_0052111 improved Fsp3 and modestly reduced logP but underwent the largest dynamic rearrangement. This discordance provides a useful negative design lesson: a favourable static score and descriptor profile may be insufficient when the substituted vector does not retain a coherent pocket interaction during simulation.

Comparison with other PFKFB3 inhibitor classes further defines the scope of the result. PFK15/PFK-158 established that pharmacological interference with PFKFB3-associated glycolysis can be advanced into oncology development [13,15], while KAN0438757 provided biochemical, structural, cellular, and target-engagement validation for a chemically distinct inhibitor [14]. The recently reported covalent inhibitors demonstrate another route to durable target engagement in pancreatic cancer models [16]. The present analogues do not supersede those classes and cannot be ranked against them without matched biochemical and cellular data. They instead test a discrete allosteric AZ67-based design strategy. Patent WO2020080979A1 illustrates that PFKFB3 intellectual-property space already includes broad families and known agents [17]; therefore, the current structures should not be described as patent-novel without a formal substructure, claim, and jurisdiction-specific analysis.

The distinction between the GNINA scoring outputs is also consequential. An empirical energy-like score and CNNaffinity are not interchangeable outputs. The former is conventionally interpreted as more favourable when more negative, whereas CNNaffinity is a positive pK prediction for which higher is better [30,31]. Reporting both fields according to their native directions preserves the observed ranking but avoids the misleading statement that a more negative 'CNN affinity' is stronger. The near-tie between MOL_0000552 and MOL_0051973 on CNNaffinity also shows why single-score ordering is fragile. Recent benchmarking has reinforced that docking performance can depend on target, chemotype, structure preparation, and evaluation design [31,41].

The molecular-dynamics results similarly require relative rather than absolute interpretation. Ligand RMSD values of 5-15 Å indicate substantial

rearrangement from the initial pose even when a trajectory reaches a plateau. MOL_0000552 can therefore be described as the least variable derivative in this dataset, not as proof of a crystallographically stable binding mode. The >30 Å transition of MOL_0052111 is more clearly inconsistent with retention of the starting pose and appropriately downgraded that compound despite its static docking predictions. MM/GBSA supported the same prioritisation, but its values are comparative approximations that simplify solvent, entropy, and sampling effects [38].

Several limitations remain. First, the study contains no PFKFB3 kinase or bisphosphatase assay, no direct binding measurement, no cellular glycolysis or viability experiment, and no assessment of anti-angiogenic activity. Second, PFKFB isoform selectivity and off-target pharmacology were not evaluated. Third, the reported 50-ns trajectories were not accompanied by independent replicate simulations, and slower pocket opening, ligand dissociation, or alternative binding modes may not be captured. Fourth, ranking may depend on grid definition, protonation and tautomer states, receptor preparation, charge assignment, force-field parameters, and solvent setup. Fifth, no active/decoy benchmark, prospective predictive-performance analysis, or co-crystal redocking RMSD was reported. Sixth, QED, logP, TPSA, and structural-alert filters are not substitutes for measured solubility, permeability, metabolic stability, pharmacokinetics, or safety. Finally, noncanonical PFKFB3 functions in brain tumours complicate a glycolysis-only interpretation [44], and tumour cells may compensate through alternative metabolic routes, including the hexosamine biosynthetic pathway [45].

The immediate experimental programme should therefore prioritise MOL_0000552 and MOL_0051973 for synthesis or procurement, chemical-identity and purity confirmation, recombinant PFKFB3 kinase and bisphosphatase assays, orthogonal binding measurements, and selectivity testing against PFKFB1, PFKFB2, and PFKFB4. Cellular studies should quantify fructose-2,6-bisphosphate, extracellular acidification, glucose uptake, lactate production, viability, apoptosis, and clonogenic survival in PFKFB3-dependent cancer models, alongside nonmalignant controls. Endothelial assays should evaluate migration, sprouting, and tube formation. Solubility, permeability, microsomal stability, cytochrome P450 liability, plasma-protein binding, and preliminary safety screens should precede *in vivo* work. Computational follow-up should include explicit enumeration of protonation/tautomer states, crystallographic redocking, active/decoy benchmarking, longer replicate simulations, and free-energy methods capable of testing the proposed substituent series.

CONCLUSION

Reaction-driven redesign of AZ67 produced a large virtual library and, after a transparently reconstructed filtration and multi-objective workflow, identified three distinct allosteric-modulator hypotheses. The selected compounds did not uniformly improve drug-like properties: lower logP and higher Fsp3 were accompanied by higher molecular weight and TPSA and lower QED. Under GNINA's native scoring conventions, MOL_0000552 had an empirical docking score of -7.55 kcal/mol and CNNaffinity of 8.18 pK, showed the least variable derivative trajectory, and produced the most favourable MM/GBSA profile. MOL_0051973 was a secondary lead, whereas MOL_0052111 was downgraded after a major dynamic rearrangement. MOL_0000552 should therefore be regarded as a prioritised computational hypothesis for biochemical and cellular testing, not as a validated PFKFB3 inhibitor or anticancer therapeutic.

ETHICS APPROVAL AND CONSENT TO PARTICIPATE

Not applicable. This study used only in silico computational modelling and did not involve human participants, animals, biological specimens, or clinical records.

CONSENT FOR PUBLICATION

Not applicable.

DATA AVAILABILITY STATEMENT

The compound-summary data, tables, and trajectory-derived figures analysed in this study are included in the manuscript and accompanying tables-and-figures file. Additional structure files, docking outputs, and trajectory-derived data can be requested from the corresponding author, subject to file-size and software-licensing restrictions.

DECLARATION OF CONFLICTING INTEREST

The authors declare no relevant financial or non-financial competing interests.

FUNDING

This research received no specific grant from any funding agency in the public, commercial, or not-for-profit sectors.

AUTHOR CONTRIBUTIONS

A.M.M. (Aeshah Muhana Mohammed): Conceptualisation, methodology, software, formal analysis, investigation, data curation, visualisation, project administration, writing—original draft, and writing—review and editing. J.K.T.A.-I. (Jameelah Kadhim Taher Al-Isawi): Methodological review, interpretation of results, intellectual contribution, and writing—review and editing. M.K.A. (Muqdad Khamis Abd): Interpretation of results, scientific discussion, supervision, and writing—review and editing. All authors reviewed and approved the final manuscript and agree to be accountable for the integrity and accuracy of the work.

ACKNOWLEDGEMENTS

No specific acknowledgements are reported.

REFERENCES

[1] Hanahan D. Hallmarks of cancer: new dimensions. Cancer Discov 2022; 12(1): 31-46. https://doi.org/10.1158/2159-8290.CD-21-1059

[2] Liberti MV, Locasale JW. The Warburg effect: how does it be-nefit cancer cells? Trends Biochem Sci 2016; 41(3): 211-218. https://doi.org/10.1016/j.tibs.2015.12.001

[3] Yalcin A, Telang S, Clem B, Chesney J. Regulation of glucose metabolism by 6-phosphofructo-2-kinase/fructose-2,6-bisphosphatases in cancer. Exp Mol Pathol 2009; 86(3): 174-179. https://doi.org/10.1016/j.yexmp.2009.01.003

[4] Okar DA, Manzano A, Navarro-Sabate A, Riera L, Bartrons R, Lange AJ. PFK-2/FBPase-2: maker and breaker of the essential biofactor fructose-2,6-bisphosphate. Trends Biochem Sci 2001; 26(1): 30-35. https://doi.org/10.1016/S0968-0004(00)01699-6

[5] Yalcin A, Clem BF, Imbert-Fernandez Y, *et al*. 6-Phosphofructo-2-kinase (PFKFB3) promotes cell-cycle progression and suppresses apoptosis via Cdk1-mediated phosphorylation of p27. Cell Death Dis 2014; 5: e1337. https://doi.org/10.1038/cddis.2014.292

[6] Chen L, Xu YX, Ren YY, *et al*. PFKFB3 as a multifaceted driver and therapeutic target in castration-resistant prostate cancer. Cell Death Dis 2025; 16(1): 760. https://doi.org/10.1038/s41419-025-08089-8

[7] De Bock K, Georgiadou M, Schoors S, *et al*. Role of PFKFB3-driven glycolysis in vessel sprouting. Cell 2013; 154(3): 651-663. https://doi.org/10.1016/j.cell.2013.06.037

[8] Schoors S, De Bock K, Cantelmo AR, *et al*. Partial and transient reduction of glycolysis by PFKFB3 blockade reduces pathological angiogenesis. Cell Metab 2014; 19(1): 37-48. https://doi.org/10.1016/j.cmet.2013.11.008

[9] Boyd S, Brookfield JL, Critchlow SE, *et al*. Structure-based design of potent and selective inhibitors of the metabolic kinase PFKFB3. J Med Chem 2015; 58(8): 3611-3625. https://doi.org/10.1021/acs.jmedchem.5b00352

[10] Emini Veseli B, Van Wielendaele P, Delibegovic M, Martinet W, De Meyer GRY. The PFKFB3 inhibitor AZ67 inhibits angiogenesis independently of glycolysis inhibition. Int J Mol Sci 2021; 22(11): 5970. https://doi.org/10.3390/ijms22115970

[11] Macut H, Hu X, Tarantino D, *et al*. Tuning PFKFB3 bisphosphatase activity through allosteric interference. Sci Rep 2019; 9(1): 20333. https://doi.org/10.1038/s41598-019-56708-0

[12] Cruz E, Bessières B, Magistretti P, Alberini CM. Differential role of neuronal glucose and PFKFB3 in memory formation during development. Glia 2022; 70(11): 2207-2231. https://doi.org/10.1002/glia.24248

[13] Clem BF, O'Neal J, Tapolsky G, *et al*. Targeting 6-phosphofructo-2-kinase (PFKFB3) as a therapeutic strategy against cancer. Mol Cancer Ther 2013; 12(8): 1461-1470. https://doi.org/10.1158/1535-7163.MCT-13-0097

[14] Gustafsson NMS, Farnegardh K, Bonagas N, *et al*. Targeting PFKFB3 radiosensitizes cancer cells and suppresses homologous recombination. Nat Commun 2018; 9(1): 3872. https://doi.org/10.1038/s41467-018-06287-x

[15] Redman R, Pohlmann P, Kurman MR, *et al*. PFK-158, first-in-man and first-in-class inhibitor of PFKFB3/glycolysis: a phase I, dose-escalation, multi-centre study in patients with advanced solid malignancies. Cancer Res 2015; 75(15 Suppl): CT206. https://doi.org/10.1158/1538-7445.AM2015-CT206

[16] Fiore A, Scarano A, Antonini G, *et al*. First-in-class covalent inhibitors of PFKFB3: discovery and characterization in PDAC models. J Med Chem 2026; 69(11): 13248-13271. https://doi.org/10.1021/acs.jmedchem.6c00235

[17] Fedichev PO, Greenman K, Chang CT, *et al*. PFKFB3 inhibitors and their uses. International patent WO2020080979A1. Published April 23, 2020.

[18] Lovering F, Bikker J, Humblet C. Escape from flatland: increasing saturation as an approach to improving clinical success. J Med Chem 2009; 52(21): 6752-6756. https://doi.org/10.1021/jm901241e

[19] Mouchlis VD, Afantitis A, Serra A, *et al*. Advances in de novo drug design: from conventional to machine learning methods. Int J Mol Sci 2021; 22(4): 1676. https://doi.org/10.3390/ijms22041676

[20] Hoffer L, Charifi-Hoareau G, Barelier S, Betzi S, Miller T, Morelli X, Roche P. ChemoDOTS: a web server to design chemistry-driven focused libraries. Nucleic Acids Res 2024; 52(W1): W461-W468. https://doi.org/10.1093/nar/gkae326

[21] Hartenfeller M, Eberle M, Meier P, *et al*. A collection of robust organic synthesis reactions for in silico molecule design. J Chem Inf Model 2011; 51(12): 3093-3098. https://doi.org/10.1021/ci200379p

[22] Veber DF, Johnson SR, Cheng HY, Smith BR, Ward KW, Kopple KD. Molecular properties that influence the oral bioavailability of drug candidates. J Med Chem 2002; 45(12): 2615-2623. https://doi.org/10.1021/jm020017n

[23] Baell JB, Holloway GA. New substructure filters for removal of pan-assay interference compounds (PAINS) from screening libraries and for their exclusion in bioassays. J Med Chem 2010; 53(7): 2719-2740. https://doi.org/10.1021/jm901137j

[24] Brenk R, Schipani A, James D, *et al*. Lessons learnt from assembling screening libraries for drug discovery for neglected diseases. ChemMedChem 2008; 3(3): 435-444. https://doi.org/10.1002/cmdc.200700139

[25] Deb K, Pratap A, Agarwal S, Meyarivan T. A fast and elitist multiobjective genetic algorithm: NSGA-II. IEEE Trans Evol Comput 2002; 6(2): 182-197. https://doi.org/10.1109/4235.996017

[26] Bickerton GR, Paolini GV, Besnard J, Muresan S, Hopkins AL. Quantifying the chemical beauty of drugs. Nat Chem 2012; 4(2): 90-98. https://doi.org/10.1038/nchem.1243

[27] Bajusz D, Racz A, Heberger K. Why is Tanimoto index an appropriate choice for fingerprint-based similarity calculations? J Cheminform 2015; 7: 20. https://doi.org/10.1186/s13321-015-0069-3

[28] Berman HM, Westbrook J, Feng Z, *et al*. The Protein Data Bank. Nucleic Acids Res 2000; 28(1): 235-242. https://doi.org/10.1093/nar/28.1.235

[29] Halgren TA. Merck molecular force field. I. Basis, form, scope, parameterization, and performance of MMFF94. J Comput Chem 1996; 17(5-6): 490-519. https://doi.org/10.1002/(SICI)1096-987X(199604)17:5/6<490::AID-JCC1>3.0.CO;2-P

[30] McNutt AT, Francoeur P, Aggarwal R, *et al*. GNINA 1.0: molecular docking with deep learning. J Cheminform 2021; 13(1): 43. https://doi.org/10.1186/s13321-021-00522-2

[31] McNutt AT, Li Y, Meli R, Aggarwal R, Koes DR. GNINA 1.3: the next increment in molecular docking with deep learning. J Cheminform 2025; 17(1): 28. https://doi.org/10.1186/s13321-025-00973-x

[32] Bowers KJ, Chow E, Xu H, Dror RO, Eastwood MP, Gregersen BA, Klepeis JL, Kolossvary I, Moraes MA, Sacerdoti FD, Salmon JK, Shan Y, Shaw DE. Scalable algorithms for molecular dynamics simulations on commodity clusters. In: Proceedings of the 2006 ACM/IEEE Conference on Supercomputing (SC '06). New York: Association for Computing Machinery 2006. Article 84. https://doi.org/10.1145/1188455.1188544

[33] Berendsen HJC, Postma JPM, van Gunsteren WF, Hermans J. Interaction models for water in relation to protein hydration. In: Pullman B, editor. Intermolecular Forces. Dordrecht: Springer 1981. p. 331-342. https://doi.org/10.1007/978-94-015-7658-1_21

[34] Lu C, Wu C, Ghoreishi D, *et al*. OPLS4: improving force-field accuracy on challenging regimes of chemical space. J Chem Theory Comput 2021; 17(7): 4291-4300. https://doi.org/10.1021/acs.jctc.1c00302

[35] Martyna GJ, Klein ML, Tuckerman M. Nose-Hoover chains: the canonical ensemble via continuous dynamics. J Chem Phys 1992; 97(4): 2635-2643. https://doi.org/10.1063/1.463940

[36] Martyna GJ, Tobias DJ, Klein ML. Constant pressure molecular dynamics algorithms. J Chem Phys 1994; 101(5): 4177-4189. https://doi.org/10.1063/1.467468

[37] Ertl P, Rohde B, Selzer P. Fast calculation of molecular polar surface area as a sum of fragment-based contributions and its application to the prediction of drug transport properties. J Med Chem 2000; 43(20): 3714-3717. https://doi.org/10.1021/jm000942e

[38] Genheden S, Ryde U. The MM/PBSA and MM/GBSA methods to estimate ligand-binding affinities. Expert Opin Drug Discov 2015; 10(5): 449-461. https://doi.org/10.1517/17460441.2015.1032936

[39] McInnes L, Healy J, Saul N, Grossberger L. UMAP: Uniform Manifold Approximation and Projection. J Open Source Softw 2018; 3(29): 861. https://doi.org/10.21105/joss.00861

[40] Nicolaou CA, Brown N. Multi-objective optimisation methods in drug design. Drug Discov Today Technol 2013; 10(3): e427-e435. https://doi.org/10.1016/j.ddtec.2013.02.001

[41] Quiroga R, Villarreal MA. Developing generalizable scoring functions for molecular docking: challenges and perspectives. Curr Med Chem 2025; 32(28): 5960-5972. https://doi.org/10.2174/0109298673334469241017053508

[42] Ballatore C, Huryn DM, Smith AB 3rd. Carboxylic acid (bio)isosteres in drug design. ChemMedChem 2013; 8(3): 385-395. https://doi.org/10.1002/cmdc.201200585

[43] Kumari S, Carmona AV, Tiwari AK, Trippier PC. Amide bond bioisosteres: strategies, synthesis, and successes. J Med Chem 2020; 63(21): 12290-12358. https://doi.org/10.1021/acs.jmedchem.0c00530

[44] Alvarez R, Mandal D, Chittiboina P. Canonical and non-canonical roles of PFKFB3 in brain tumors. Cells 2021; 10(11): 2913. https://doi.org/10.3390/cells10112913

[45] Akella NM, Ciraku L, Reginato MJ. Fueling the fire: emerging role of the hexosamine biosynthetic pathway in cancer. BMC Biol 2019; 17(1): 52. https://doi.org/10.1186/s12915-019-0671-3

Received on 29-07-2026 Accepted on 24-08-2026 Published on 27-08-2026

https://doi.org/10.30683/1929-2279.2026.15.23